Electronic Supplementary Information (ESI)

Exciton Funneling Amplified Photoluminescence Anisotropy in Organic Radical-Doped Microcrystals

Zhonghao Zhou, Chan Qiao, Jiannian Yao, Yongli Yan* and Yong Sheng Zhao*

CAS Key Laboratory of Photochemistry, Institute of Chemistry, Chinese Academy of Sciences, Beijing 100190, China

*Corresponding author: ylyan@iccas.ac.cn; yszhao@iccas.ac.cn.

Contents

9. **Figure S7.** Concentration-dependent PL decay profiles of PyBTM-doped *αH*-PyBTM microcrystals monitored at 570 nm.

10. **Table S2.** Efficiency of energy transfer in PyBTM-doped *αH*-PyBTM microcrystals.

11. **Figure S8.** Schematic illustration of the experimental setup for optical characterization.

12. **Figure S9.** Transition dipole moments of *αH*-PyBTM and PyBTM.

13. **Figure S10.** Temperature-dependent PL decay profiles of PyBTM-doped *αH*-PyBTM microcrystals monitored at 570 nm.

14. **Figure S11.** Temperature-dependent PL spectra of an identical PyBTM-doped microcrystal.

Experimental details

Materials:

Starting materials of (3,5-dichloro-4-pyridyl)bis(2,4,6-trichlorophenyl)methyl (PyBTM) and *αH*-PyBTM. 3,5-Dichloro-isonicotinaldehyde (97%), 1,3,5-trichloro- benzene (99%), Trifluoromethanesulfonic acid (99%), t-BuOK (99%) and Iodine (99.8%) were purchased from Innochem (Beijing, China) and used to synthesize *αH*-PyBTM and PyBTM according to a previous study.[1]

Other material. Polystyrene (PS, M.W. 260,000) purchased from InnoChem (Beijing, China) was selected as the matrix material to investigate the optical stability of PyBTM.

Preparations:

Preparation of 1 wt% PyBTM:PS film. PyBTM-doped PS films were prepared by drop-casting from PyBTM/PS/CH_2Cl_2 solution. First, 0.1 mg of PyBTM and 10.0 mg of PS were dissolved in 1.0 mL of CH_2Cl_2 under stirring. Then, the solution was drop-cast onto quartz wafers in air. After total evaporation of CH_2Cl_2, 1 wt% PyBTM:PS films (116 ± 7 μm) were obtained.

Preparation of the light-harvesting PyBTM doped *αH*-PyBTM microcrystals. The light-harvesting microcrystals were prepared with solvent evaporation–induced self-assembly. In a typical preparation, 25 μL of 10 mM *αH*-PyBTM in acetonitrile was first mixed with 25 μL of PyBTM acetonitrile solution to form a homogeneous mixture, which was then placed in a 20-mL closed beaker containing 3.0 mL of methanol anti-solvent. In the whole procedure, a

solvent atmosphere was kept and the evaporation speed of the solvent (i.e., the saturation degree of the solution) was well controlled. A large number of doped microcrystals were finally obtained after 18 hours. The PyBTM doping concentrations in *αH*-PyBTM were adjusted by changing the concentration of PyBTM acetonitrile solution. The actual doping concentrations of PyBTM in light-harvesting microcrystals were determined according to reference.[2]

Stimulations:

The electronic transition dipole moment (μ) of *αH*-PyBTM and PyBTM was calculated by time-dependent density functional theory carried out in Gaussian 09 package using the B3LYP hybrid functional. The electronic structures were optimized using 6-311G** basis set.

Characterizations:

Morphological characterization. The morphology of the prepared microcrystals was examined with a scanning electron microscope (Hitachi, S-4800) and a transmission electron microscope (JEOL, JEM-2100). Powder X-ray diffractions were performed on the Rigaku D/max-2500 instrument (Cu Kα, 1.54 Å). Single crystal data of *αH*-PyBTM was obtained on a R-AXIS RAPID IP X-ray diffractometer (Rigaku, Japan) with graphite-monochromated Mo–Kα radiation (λ = 0.71073 Å).

Photoluminescence quantum yield characterization. The photoluminescence quantum yield (PLQY) measurements were performed using an absolute method on Quantaurus-QY C11347 (Hamamatsu). In a typical measurement, a clean, empty silica dish was set as

reference to calibrate the instrument at first. After calibration, PyBTM-doped *αH*-PyBTM microcrystals with various doping concentration were transferred into the silica dish and excited with a light-emitting diode at a wavelength of 405 nm. Between each measurement, the dish was carefully washed with dichloromethane. The absolute PLQYs were calculated by comparing the integral of the emission and the absorption of excited light.

Other optical characterizations. The fluorescence spectra were measured using a Hitachi F-7000. The absorption spectra were measured using a Hitachi UH-4150. The photoluminescence (PL) decay profiles were obtained base on Hamamatsu Quantaurus-Tau C11367. The morphology of the prepared PyBTM doped *αH*-PyBTM microcrystals was examined by laser confocal fluorescence microscopy (Olympus FV1000-IX81) equipped with 405 nm continusous-wave laser. Bright-field and fluorescence microscopy images were acquired using an inverted fluorescence microscope (Nikon, Ti-U) under the excitation of a mercury lamp (330-380 nm). The PL anisotropy measurements for individual microcrystals were conducted on a custom micro-PL system shown in Figure S8.

Table S1. Crystallographic data of *αH*-PyBTM.

Compound	*αH*-PyBTM
Empirical formula	$C_{18}H_7Cl_8N$
CCDC number	2093989
Formula weight	520.88
Crystal system	Triclinic
Space group	*P*-1
a (Å)	8.311 (4)
b (Å)	9.782 (4)
c (Å)	13.289 (5)
α (deg)	92.425 (6)
β (deg)	106.857 (6)
γ (deg)	105.539 (3)
Volume ($Å^3$)	987.685
Z	2
R factor (%)	7.11

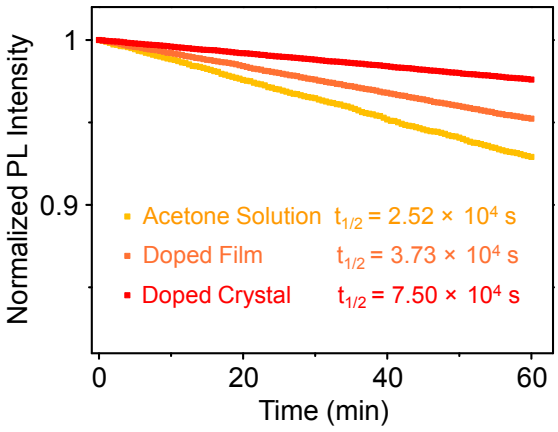

Figure S1. Plots of PL intensity of PyBTM as a function of excitation time in different systems. The concentrations of PyBTM are 1.1 wt%, 1.0 wt% and 0.1 mM in doped crystals, doped film and acetone solution, respectively.

The photostability of the luminescent organic raidicals is curical for their applications.[1] The photostability of PyBTM doped *αH*-PyBTM microcrystals was evaluated and comparied with that in soultion and amorphous film. When the samples were irradiated at λ = 375 nm, the degradation of the PL intensity of PyBTM in doped crystals was 3 times and 2 times smaller than those in acetone solution and polystrene film, respectively (Figure S1). This excellent photostability of PyBTM doped *αH*-PyBTM microcrystals results from the rigid environments provided by the dense packing *αH*-PyBTM matrix.

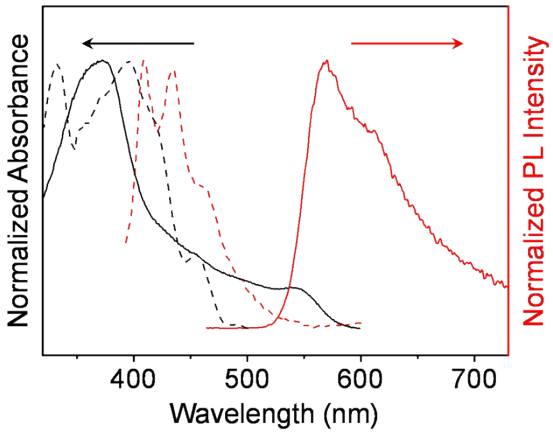

Figure S2. Normalized absorption and PL spectra of αH-PyBTM microcrystals (dash lines) and 1.0 wt% PyBTM-doped polystyrene film (solid lines).

As shown in Figure S2, the αH-PyBTM microcrystals show broadband absorption in the ultraviolet-to-blue region, which can efficiently harvest excitation light. Moreover, the large spectroscopic overlap between the emission spectrum of αH-PyBTM and absorption spectrum of PyBTM facilitates the energy transfer from host crystals to guest molecules.

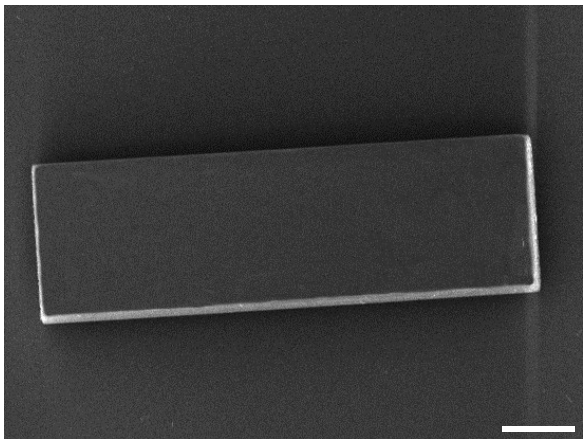

Figure S3. Scanning electron microscopy image of an individual pure *αH*-PyBTM microcrystal. Scale bar is 5 μm.

As shown in Figure S3, the pure *αH*-PyBTM microcrystal has a well-defined rectangular morphology with smooth facets, implying the high quality of the as-prepared microcrystal.

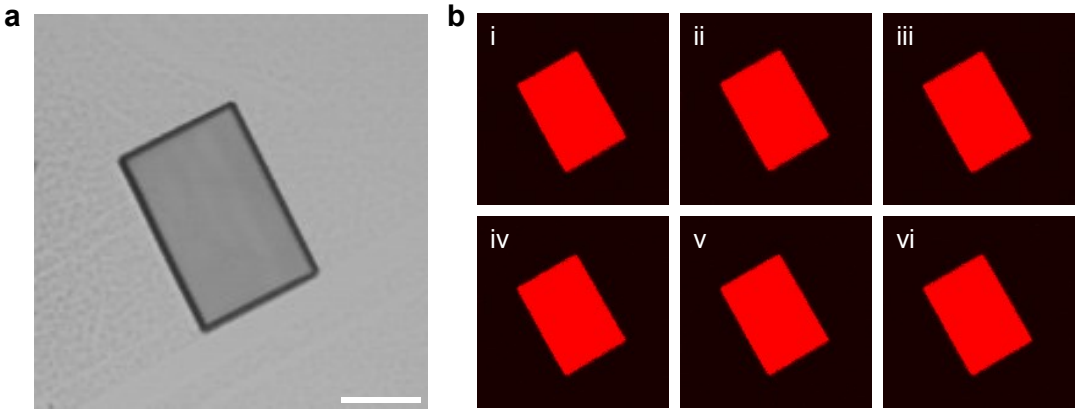

Figure S4. Confocal microscopy images of a typical PyBTM-doped *αH*-PyBTM microcrystal. (a) Bright-field image of a PyBTM doped *αH*-PyBTM microplate. Scale bar is 10 μm. (b) Confocal PL images (emission band, 580-680 nm) collected at different focal planes with interplane distance of 300 nm.

As displayed in Figure S4a, the bright-field image of the as-prepared PyBTM-doped *αH*-PyBTM crystal shows a well-defined microplate structure. The corresponding PL images of PyBTM-doped *αH*-PyBTM microcrystal in Figure S4b at different focal planes exhibit the same morphology with uniform red PL emission from i to vi, indicating that PyBTM molecules are uniformly dispersed in the *αH*-PyBTM matrices.

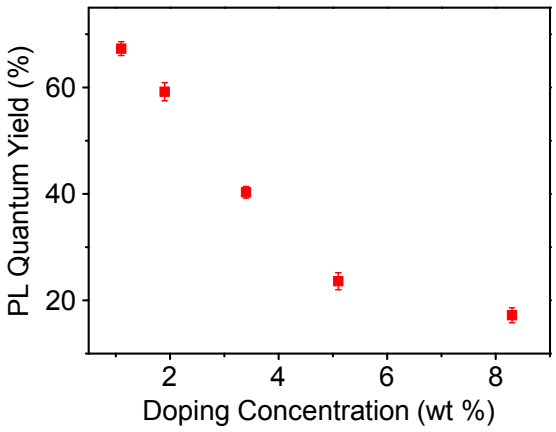

Figure S5. Concentration-dependent PL quantum yields of PyBTM-doped *αH*-PyBTM microcrystals.

Figure S5 shows PL quantum yields of PyBTM doped *αH*-PyBTM microcrystals with different doping concentrations. When doping concentration is relatively low, the emission of doped microcrystals is dominant by PyBTM monomer emission. The PL quantum yields decrease sharply with increasing concentration, which should be attributed to the long-distance non-radiative deactivation processes among isolated PyBTM molecules.[2] As the radical concentration further increases, the PL quantum yield of microcrystals decreases gradually along with enhanced emission located at ~680 nm, showing a typical characteristic of excimer emission.

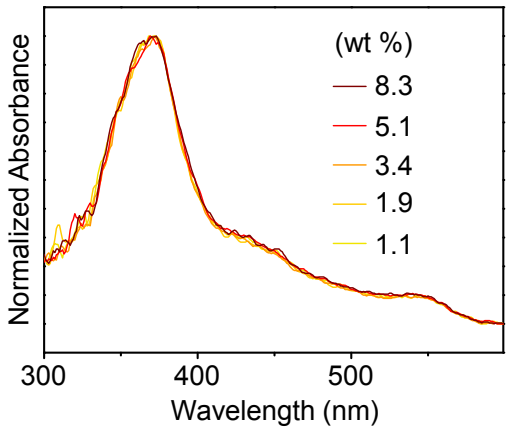

Figure S6. Concentration-dependent absorption spectra of the PyBTM-doped *αH*-PyBTM microcrystals.

Although a distinct PL peak appeared at ~680 nm with increasing PyBTM concentration in host crystals (Figure 2b), almost no change was found in the absorption spectra (Figure S6). These features are in good accordance with the generation of excimers originating from the association of an excited molecule and an unexcited molecule,[3,4] which are only stable in excited state and repulsive with each other in the ground state.

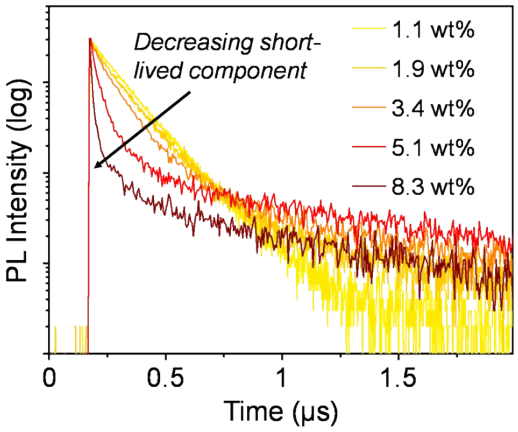

Figure S7. Concentration-dependent PL decay profiles of PyBTM-doped *αH*-PyBTM microcrystals monitored at 570 nm.

The decrease of the short-lived component of PL lifetime monitored at 570 nm becomes rapider as the concentration of PyBTM in host crystals increases (Figure S7), implying a strong quenching of the monomer emission. Moreover, the increasing PyBTM concentration would shorten the average inter-chromophore distance, facilitating the energy migration from monomers to excimers.[5]

Table S2. Efficiency of energy transfer in PyBTM-doped *αH*-PyBTM microcrystals.

c (wt%)	t_1 (ns)	w_1 (%)	t_2 (ns)	w_2 (%)	t_3 (ns)	w_3 (%)	t_{cor} (ns)	χ^2	E_{ET} (%)
1.1	124.40	77.93	215.18	22.07	/	/	144.43	1.07	78
8.3	8.97	42.55	85.05	18.69	886.37	38.76	32.19	1.01	

The PL decay curves at 570 nm of 1.1 wt% and 8.3 wt% PyBTM-doped microcrystals in Figure S7 were fitted to multiple exponential function $I = A \times (w_1 e^{-t/t1} + w_2 e^{-t/t2} + \cdots)$, where I is the fluorescence intensity and A is the intensity constant, respectively. Because the long-lived component of the PL lifetime in 8.3 wt% doped crystals (886.37 ns of t_3, Table S1) should be attributed to the interference of excimer emission at 570 nm,[6] the corrected average lifetime t_{cor} could be approximately calculated according to the formula $t_{cor} = (w_1 t_1 + w_2 t_2)/(w_1 + w_2)$. The corresponding efficiency of energy transfer was calculated according to $E = 1 - t_{DA}/t_D$, where t_{DA} is the corrected average lifetime of doped microcrystals in presence of excimers (32.19 ns of the 8.3 wt% doped microcrystals), and t_D is the average lifetime of doped microcrystals in the absence of excimers (144.43 ns of the 1.1 wt% doped microcrystals), respectively. The efficiency of energy transfer was estimated to be 78%, which is high enough for efficient exciton funneling in excimers for PL anisotropy amplification.

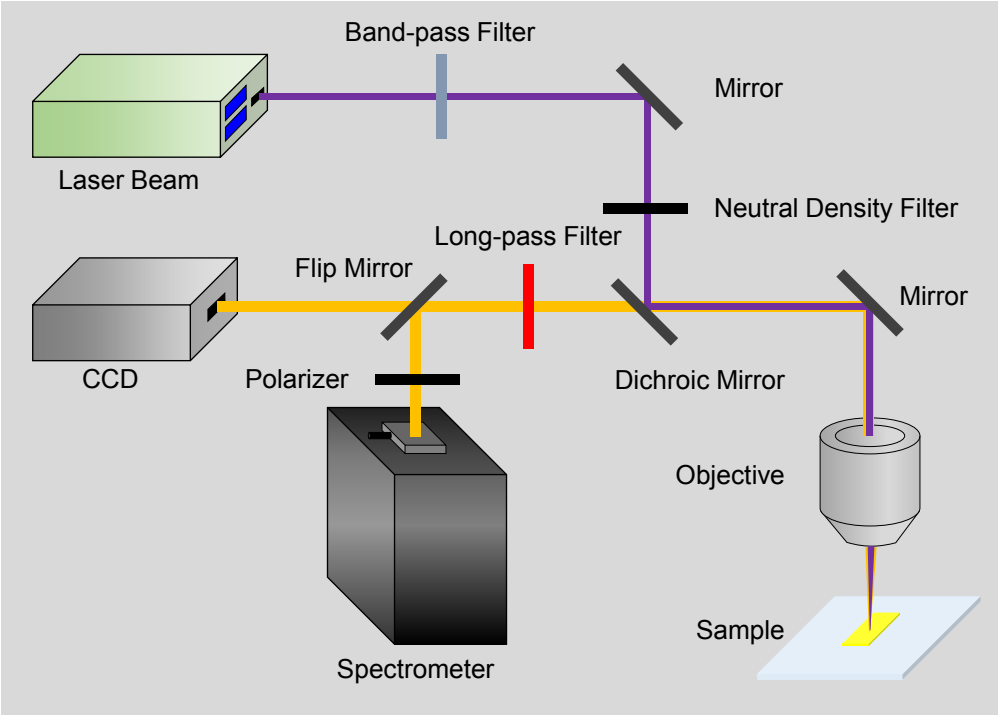

Figure S8. Schematic illustration of the experimental setup for optical characterization.

A homemade micro-PL system was used to study the PL anisotropic properties of the PyBTM-doped *αH*-PyBTM microcrystals (Figure S8). The crystals were excited locally with a 375 nm continuous-wave laser filtered by 357/44 nm band-pass filter. The plate like microcrystals on glass substrates (refractive index ~1.5) were locally excited with the laser beam focused down to ~7 μm in diameter through an objective (Nikon CFLU Plan, 50×, N.A. = 0.8), with input power altered by neutral density filters. The polarization orientation of the laser source was parallel to the transition dipole moment of the microcrystals. After passing through a 420 nm long-pass emission filter, polarized PL signals were modulated by rotating the polarizer in front of the spectrometer, and subsequently coupled to a grating spectrometer (Acton SP-2358) connected with a thermal-electrically cooled CCD (Princeton Instruments, ProEm: 1600B). For the temperature-dependence measurements, the samples were placed in a cryostat (M-22, Janis) equipped with a telephoto objective lens (Olympus LMPLFLN, 50 ×, N.A. = 0.5).

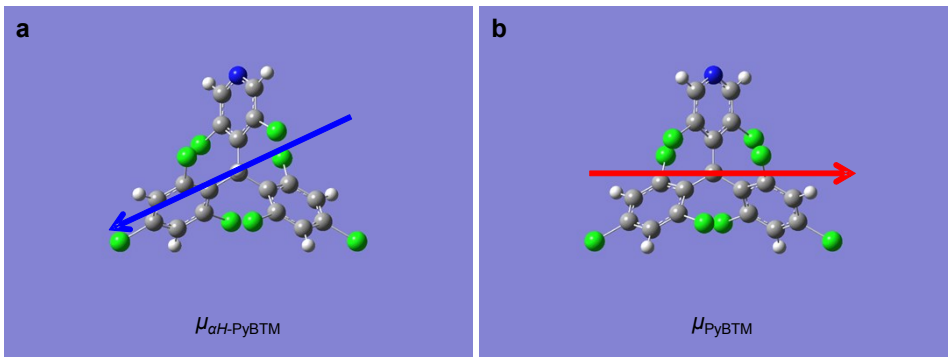

Figure S9. Transition dipole moments of *αH*-PyBTM (blue arrow, a) and PyBTM (red arrow, b).

As shown in Figure S9, although the direction of μ in PyBTM molecule is different from that in *αH*-PyBTM molecule, the polarized orientation of PL emission from PyBTM is consistent with that in *αH*-PyBTM in doped crystals, which indicates that the μ of PyBTM is aligned paralleled to that of host molecules under dense packing.

a

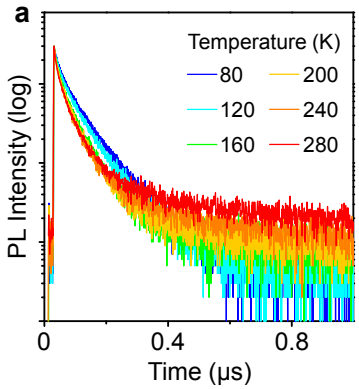

b

T (K)	τ_1 (ns)	w_1 (%)	τ_2 (ns)	w_2 (%)	τ_3 (ns)	w_3 (%)	τ_{cor} (ns)	χ^2
80	25.72	28.22	87.46	71.78	/	/	70.04	1.26
120	27.09	34.35	85.67	65.65	/	/	65.55	1.20
160	13.78	18.32	51.59	70.75	210.09	10.93	43.81	1.19
200	12.08	15.77	46.72	69.55	200.35	14.67	40.32	1.05
240	16.87	23.24	46.55	54.79	506.25	21.97	37.71	1.17
280	18.82	22.96	41.85	45.09	660.34	31.95	34.08	1.12

Figure S10. Temperature-dependent PL decay profiles of PyBTM-doped *αH*-PyBTM microcrystals monitored at 570 nm. (a) PL decay profiles of PyBTM-doped *αH*-PyBTM microcrystals at 570 nm at various temperatures. (b) Corresponding PL decay characteristics of the microcrystals extracted from (a).

As temperature increases, both the value and proportion of short-lived lifetime components monitored at 570 nm decreases gradually (Figure S10), which implies an efficient quenching of monomer emission and activation of the energy transfer between monomer and excimer states in the doped microcrystals.

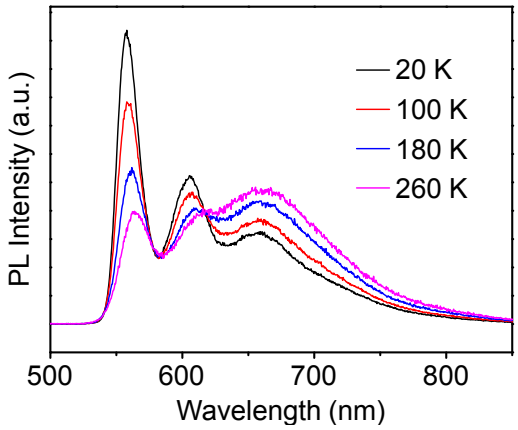

Figure S11. Temperature-dependent PL spectra of an identical PyBTM-doped microcrystal.

The broadband excimer emission located at ~680 nm became stronger with increasing temperature from 20 to 260 K (Figure S11), which clearly demonstrates that the excitation energy has been efficiently concentrated on the low-lying excimer states through energy transfer processes between monomers and excimers.

References

1. Y. Hattori, T. Kusamoto and H. Nishihara, *Angew. Chem., Int. Ed.,* 2014, **53**, 11845–11848.
2. S. Kimura, T. Kusamoto, S. Kimura, K. Kato, Y. Teki and H. Nishihara, *Angew. Chem., Int. Ed.,* 2018, **57**, 12711–12715.
3. J. B. Birks and L. G. Christophorou, *Nature,* 1962, **194**, 442–444.
4. J. B. Birks, *Nature,* 1967, **214**, 1187–1190.
5. A. J. Musser, S. K. Rajendran, K. Georgiou, L. Gai, R. T. Grant, Z. Shen, M. Cavazzini, A. Ruseckas, G. A. Turnbull, I. D. W. Samuel, J. Clark and D. G. Lidzey, *J. Mater. Chem. C,* 2017, **5**, 8380–8389.
6. M. J. Snare, P. J. Thistlethwaite and K. P. Ghiggino, *J. Am. Chem. Soc.,* 1983, **105**, 3328–3332.